# Understanding Quasi-Periodic Fieldlines and Their Topology in Toroidal Magnetic Fields

Allen Sanderson, Guoning Chen, Xavier Tricoche, and Elaine Cohen

**Abstract** In the study of a magnetic confinement fusion device such as a tokamak, physicists need to understand the topology of the flux (or magnetic) surfaces that form within the magnetic field. Among the two distinct topological structures, we are particularly interested in the magnetic island chains which correspond to the break up of the ideal rational surfaces. Different from our previous method [12], in this work we resort to the periodicity analysis of two distinct functions to identify and characterize flux surfaces and island chains. These two functions are derived from the computation of the fieldlines and puncture points on a Poincaré section, respectively. They are the *distance measure plot* and the *ridgeline plot*. We show that the periods of these two functions are directly related to the topology of the surface via a resonance detection (i.e. period estimation and the common denominators computation). In addition, we show that for an island chain the two functions possess resonance components which do not occur for a flux surface. Furthermore, by combining the periodicity analysis of these two functions, we are able to devise a heuristic yet robust and reliable approach for classifying and characterizing different magnetic surfaces in the toroidal magnetic fields.

## 1 Introduction

In magnetic confinement fusion devices such as a tokamak, magnetic fields are used to confine a burning plasma (Figure 1a). In the study of such devices, physicists need to understand the topology of the *flux surfaces* that form within the magnetic fields. Flux surfaces come in a rational and irrational form and are defined by periodic

Allen Sanderson and Guoning Chen
SCI Institute, University of Utah, Salt Lake City, UT 84112. e-mail: allen, chengu@sci.utah.edu

Xavier Tricoche
Purdue University, West Lafayette, IN 47907. e-mail: xmt@purdue.edu

Elaine Cohen
University of Utah, Salt Lake City, UT 84112. e-mail: cohen@cs.utah.edu

and quasi-periodic fieldlines, respectively. Our focus is the break up of the rational surfaces into the irrational ones, specifically those that form *magnetic island chains* because they are where the plasma escapes and will damage the wall of the fusion reactor.

To distinguish the magnetic island chains from other flux surfaces, we study their behavior in a Poincaré map computed by intersecting fieldlines with a plane perpendicular to the axis of the torus. A naive geometric test was proposed to identify different magnetic surfaces from the Poincaré section in our previous work [12]. Unfortunately, it does not make use of the periodicity properties of the flux surfaces as we will show later and hence it is computationally expensive and not reliable. In this work we describe a more robust approach that analyzes the distinct periodic behaviors of flux surfaces and island chains, which helps us achieve more efficient characterization of these two structures. More specifically, we estimate the fundamental periods of two functions stemming from the fieldline tracing and the puncture point computation, respectively. These two functions are formed via the *distance measure plot* and the *ridgeline plot*. We show that the periods of these two functions, when coupled are directly related to the topology of a surface. We should note that in our previous work we have described the ridgeline plot but only used it to complement the geometric test. With the addition of the distance measure plot we are now able to couple them together to form a magnetic surface characterization framework which has a more rigorous foundation.

One of the key components in the classification of rational and irrational surfaces, is the *safety factor*. The safety factor is the limit of the ratio of the *winding pair*, i.e. the number of times a fieldline traverses around the major axis of the torus (toroidal winding) for each traversal around the minor axis of the torus (poloidal winding) (Figure 1b). Although based on the above description the poloidal winding may not be integer (Section 4), in the later discussion we consider only integer pairs for the winding pairs. Choosing a good winding pair is of paramount importance because it will determine how we connect the discrete puncture points to get the contiguous representation of the surfaces [12]. In what follows, we will describe in detail how we combine the results of the period estimation of the two functions and other metrics to form a heuristic framework and obtain the desired winding pairs for both geometry construction and topological characterization of a fieldline. We will also explain how the detection of resonance components in the period analysis of an island chain can help us identify this structure in an early stage.

## 2 Related Work

Magnetic fields are described in terms of vector fields. While a rich body of visualization research has focused on the extraction of features of interest in vector fields [11, 7] starting from [6], the identification of the invariant structures such as periodic orbits from the flow is most relevant to our work.

Within the fusion community researchers have located periodic fieldlines using numerical approaches such as those by [4]. Wischgoll and Scheuermann were the first in the visualization community to present an algorithm for detecting periodic

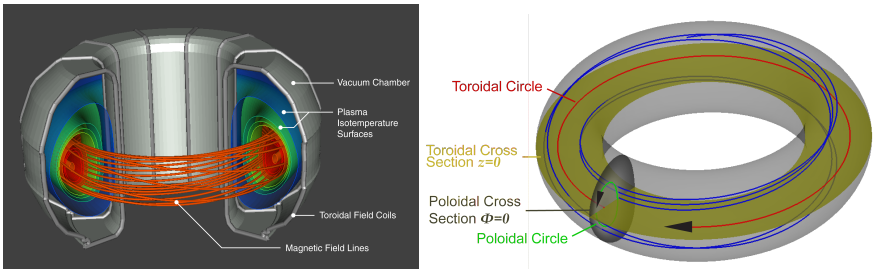


(a) (b)

Fig. 1: (a) Profile of the DIII-D Tokamak and a single quasi-periodic magnetic fieldline (the red curves). (b) A magnetic fieldline (blue) that intersects the poloidal plane (gray) and the toroidal plane (gold).

orbits in planar flows [15]. Their method examines how a fieldline re-enters a cell and re-connects. They have also extended their technique to 3D vector fields [16]. In the meantime, Theisel et al. [13] presented a mesh independent approach to compute periodic orbits. Recently, Chen et al. [2] proposed an efficient algorithm to extract periodic orbits from surface flows using *Morse decompositions*.

We also note the work of Löffelmann et al. [8] who integrated 2D Poincaré plots with the original 3D flow for visualization purposes. Recently, an analysis technique for divergence free flow fields has also been proposed by Peikert and Sadlo [9, 10] who introduced a divergence cleaning scheme to study vortex breakdown flow patterns through their long-term Poincaré plot. Others have used a graph-based approach combined with the machine learning technique to classify the fieldlines [1].

## 3 Background

In this section, we briefly review some important concepts of Poincaré map and toroidal magnetic fields. More details can be found in [12].

### *3.1 Poincaré Map*

Consider a vector field $V$ on a manifold $\mathscr{M}$ (e.g. a triangulation) with dimension $n$ ($n = 3$ in this work), which can be expressed as an ordinary differential equation $\frac{dx}{dt} = V(x)$. The set of solutions to it gives rise to a *flow* $\varphi$ on $\mathscr{M}$. Let $\Gamma$ be a trajectory (integral curve) of a vector field $V$. Let $\mathscr{S}$ be a cross section of dimension $n-1$ (e.g. a plane perpendicular to the major axis of the torus) such that $\varphi$ is everywhere transverse to $\mathscr{S}$. $\mathscr{S}$ is referred to as a Poincaré section. An intersection of $\Gamma$ with $\mathscr{S}$ is called a *puncture point*, denoted by $l_i \in \mathscr{S} \cap \Gamma$ ($i \in \mathbb{N}$ shows the intersection order). The Poincaré map is defined as a mapping in $\mathscr{S}$ $P : \mathbb{R} \times \mathscr{S} \to \mathscr{S}$ that leads a puncture point $l_i$ to the next position $l_{i+1} \in \mathscr{S} \cap \Gamma$ following $\Gamma$.

### 3.2 Toroidal Magnetic Fields

A toroidal magnetic field is a 3D vector field where the magnetic fieldlines exhibit helical behavior and wind around the major (toroidal) circle and minor (poloidal) circle of the torus (Figure 1b).

The safety factor of a fieldline, $q$, is defined as the number of times a fieldline goes around the toroidal circle for each rotation around the poloidal circle, and is computed as:

$$q = \lim_{\#T \to \infty} \frac{\#T}{\#P} \tag{1}$$

where $\#T$ is the toroidal winding count (rotations about the toroidal circle) and $\#P$ is the poloidal winding count (rotations about the poloidal circle). We define the two winding counts when expressed as rational numbers as a *winding pair*. Because we cannot integrate to infinity, in practice we estimate the safety factor of a surface based on a finite number of integrations (Section 4.1).

By definition, the safety factor $q$ can be either rational or irrational. A rational $q$ implies that the fieldline is periodic (or closed in finite distance). Such a fieldline lies on a *rational surface*. Such surfaces are found in a fusion device. However, they are unstable and sensitive to the magnetic perturbation. Among them, the ones with lower-order $q$ are the first to break down into island chains [14]. Figure 2 provides an example of such a topology change of a magnetic surface due to the magnetic perturbations. An irrational $q$ implies that the fieldline is quasi-periodic. Such a fieldline lies on an *irrational surface* and spreads out over it. This type of flux surfaces is our focus in this work. They have two distinct topology shown in a Poincaré section, a single closed curve or multiple closed curves. A single closed curve typically represents a magnetic flux surface when it encloses the center of the magnetic field. Multiple closed curves represent a magnetic island chain which is usually associated with a reduction in magnetic confinement [12].

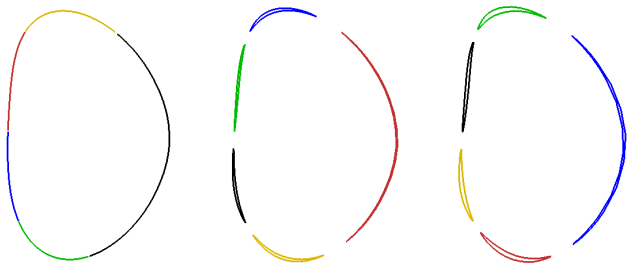

(a) (b) (c)

Fig. 2: The evolution of a magnetic surface at different times of the fusion simulation: (a) an irrational flux surface at time step 22; (b) a 5,2 island chain at time 23; (c) the growing 5,2 island chain at time 24.

There are two types of critical points for a magnetic island chain, commonly referred to as $X$ (unstable or saddle) and $O$ (stable or center) points. They correspond to the locations where there is no poloidal magnetic flux [5]. In the case of an $O$

point, it is located at the magnetic center of an island. While for an $X$ point, it is located where two flux surfaces appear to cross and form a *separatrix* around the magnetic islands. In this work, we focus on only the characterization of fieldlines. The detection of critical points can be found in [12].

According to [12], an irrational surface consists of $\#T$ winding groups in the Poincaré section. The geometrically neighboring groups need not be neighbors in the puncture point ordering. In order to construct a valid geometry representation without self-intersections for the surface, a proper winding pair is greatly desired. In the following, we describe how we achieve so.

## 4 Fieldline Puncture Points And Winding Pairs

In [12] we collected a set of puncture points at the Poincaré section while counting the numbers of the associated toroidal and poloidal windings of the fieldline. We briefly review this collection: Let $A_i$ be a tuple describing the state of each puncture point of a fieldline $\Gamma$ at the Poincaré section $\mathscr{S}$. Further, let $A_i = (l_i, \#T, \#P)$ where $l_i$ represents the location of $A_i$ in $\mathscr{S}$, $\#T$ is the number of crossing of $\Gamma$ through $\mathscr{S}$ when reaching $l_i$, and $\#P$ the number of crossing of $\Gamma$ through the toroidal cross section (the horizontal brown plane in Figure 1b) when $d(\Gamma)_z > 0$ (increasing z coordinates) and when reaching $l_i$ (see Figure 1b for an illustration).

The above gives a good estimation of the poloidal winding when the magnetic axis (the central axis of the magnetic field) is nearly planar. However, as the magnetic field is perturbed, the axis no longer lies in a plane and the above estimation fails. As such, we do a more computationally expensive continuous sampling of the poloidal winding through a rotational transform [14]:

$$\#P \approx \frac{1}{2\pi} \int_o^S ds \frac{d\theta}{ds} \, \mathrm{d}s \tag{2}$$

where $S$ is the total length that the fieldline is integrated over and $d\theta$ is the change in poloidal angle for the distance $ds$ traveled along the fieldline. Further $\frac{d\theta}{ds}$ can be defined as:

$$\frac{d\theta}{ds} = \frac{d}{ds}[arctan(\frac{Z}{R})] = (\frac{1}{R^2+Z^2})(R\frac{dZ}{ds} - Z\frac{dR}{ds}), \tag{3}$$

while in a cylindrical coordinate system. That is, we are summing up the poloidal changes along the fieldline and then dividing by the total toroidal distance traveled.

When reaching $l_i$ in the Poincaré section $\mathscr{S}$ we record $\#T$ like before (as an integer) and $\#P$ from equation 2 as a rational number (i.e. rounded to an integer). $\#P$ is stored as a rational number because we are interested in two rational values (aka a winding pair) to utilize with the fundamental periods (integers) of the distance measure plot and ridgeline plots that will be described in Section 5.

### *4.1 Safety Factor Approximation*

By definition the safety factor is the limit of the ratio of the winding numbers when the fieldline is traced infinitely long (equation 1). As noted, only a limited number of integration steps can be computed before numerical inaccuracies lead the field line to an erroneous path. As such, to approximate the safety factor we simply divide $\#T$ by $\#P$ (as a floating point value) from equation 2 for the last puncture point in $A$.

### *4.2 Ranking Winding Pairs*

In [12], we identified a single poloidal-toroidal winding pair for a value of $T$ such that

$$\min_{T\in\mathbb{N}}(d) = \sum_{i=T} \|(P_{i+T} - P_i) - (P_i - P_{i-T})\| \tag{4}$$

is minimized, where $P_i$ is the number of crossings of $\Gamma$ through the toroidal cross section plane when reaching the puncture point $l_i$. When $d$ is minimized, the toroidal winding number $\#T = T$ and the poloidal winding number $\#P = P_T$.

The minimization is based on an important observation: for a given toroidal winding number $\#T$, the poloidal winding number should be consistent between every $\#T$ puncture points. For example, if the toroidal winding number is 5 and the poloidal winding number is 2. Then the poloidal winding counts, $\#P$ could be:

$0,1,1,1,2,\ \ 2,3,3,3,4,\ \ 4,5,5,5,6$

In this case the difference between every $5^{th}$ value (the toroidal winding number) is 2 (the poloidal winding number).

While the minimization results in one "best" winding pair there are multiple possible winding pairs, each of which is a *rational approximation* to the irrational safety factor. In our previous work [12] we were only interested in the "best" winding pair while in the present work we are interested in multiple pairs. In Table 1 we show the possible pairs for an irrational surface ranked based on the minimization criteria in equation 4. For this criterion, a 29,11 surface would be the best candidate.

It is also possible to rank the winding pairs based on other criteria. For example, the 29,11 pair results in a safety factor of 2.63636 which is not the best approximation given the safety factor of 2.6537 as calculated using the rotational sum. As such, selecting the winding pair that is closest to the approximated safety factor is another option. In Table 2, we rank the winding pairs based on this criterion. In this case, the 61,23 surface would be the closest match while the 29,11 surface would now be ranked sixth. However, the winding pair we seek should provide us information for the geometry reconstruction. The winding pairs obtained using the above two criteria could not be proven to contain such information. Therefore, in the following we turn to the analysis of two functions, the distance measure plot and ridgeline plot.

Table 1: Winding pairs using 125 puncture points, 48 ridgeline points with a base safety factor of 2.6537 ranked based on the best matching pair consistency.

| Toroidal/Poloidal Winding Pair | Safety Factor | Equation 4 (Normalized) |
|---|---|---|
| 29, 11 | 2.63636 | 98.9583 |
| 37, 14 | 2.64286 | 98.8636 |
| 8, 3 | 2.66667 | 97.4359 |
| 45, 17 | 2.64706 | 96.25 |
| 21, 8 | 2.625 | 95.1923 |
| 50, 19 | 2.63158 | 93.3333 |
| 53, 20 | 2.65 | 93.0556 |
| 13, 5 | 2.6 | 91.9643 |
| 61, 23 | 2.65217 | 90.625 |

Table 2: Winding pairs using 125 puncture points and 47 ridgeline points with a base safety factor of 2.6537 ranked based on the best rational approximation.

| Toroidal/Poloidal Winding Pair | Safety Factor | Best Rational Approximation |
|---|---|---|
| 61, 23 | 2.65217 | 0.00152259 |
| 45, 17 | 2.64706 | 0.00663767 |
| 53, 20 | 2.65 | 0.0036965 |
| 37, 14 | 2.64286 | 0.0108394 |
| 8, 3 | 2.66667 | 0.0129702 |
| 29, 11 | 2.63636 | 0.0173329 |
| 50, 19 | 2.63158 | 0.0221176 |
| 21, 8 | 2.625 | 0.0286965 |
| 13, 5 | 2.6 | 0.0536965 |

## 5 Distance Measure Plot and Ridgeline Plot

In this section, we describe the distance measure and ridgeline plots whose periods are dependent on the toroidal and the poloidal periods, respectively. To obtain their periods and subsequently the classification of the fieldlines, we perform a period analysis. Unlike the safety factor and winding pair analysis which required both the toroidal and poloidal windings, the period analysis of each plot is independent.

### *5.1 Distance Measure Plot*

We introduce a distance measure that is defined as the distance between two puncture points:

$$d_i = \|l_{i+T} - l_i\| \tag{5}$$

where $T$ is the interval between two puncture points.

When the fieldline is periodic (i.e. lies on a rational surface) and has a toroidal period of $T$, $d_i$ between every $T$ points will be zero. When the fieldline is quasi-periodic (i.e. lies on an irrational surface) $d_i$ will be non zero for all points in $A$ (Figure 3). But the sum of distances is minimal when $T$ is the toroidal winding period. This is equivalent to finding the period $T$ that minimizes the following:

$$\min_{T\in\mathbb{N}}(d) = \sum_{i=T} \|l_{i+T} - l_i\| \tag{6}$$

One can interpret equation 6 as the solution to a minimum spanning tree where the points are the nodes and the weights of the edges are the distances between the points, $d_i$.

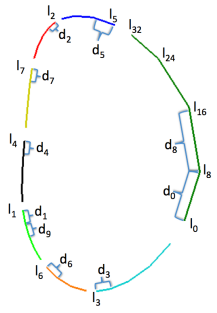


Fig. 3: An 8,3 flux surface with the puncture points, $l_i$ and the distances, $d_i$ between each eighth puncture point.

While perhaps not obvious one can look at each interval $T$ as the basis for a 1D plot where the sample values are the distances from equation 5 (thus the term distance measure plot). Figure 5 (b) and (d) show two distance measure plots with $T$ equal the fundamental periods where the sum of the distances are minimized.

## *5.2 Ridgeline Plot*

Previously [12], we noted that for each poloidal winding in the fieldline there is a local maximum, $r$ with respect to the toroidal cross section (i.e the $Z = 0$ plane), which is defined as:

$$\Gamma_z(r) > 0; \frac{\partial \Gamma(r)}{\partial z} = 0. \tag{7}$$

The *ridgeline plot* is defined as the collection of these local maxima.

It is easy to understand the construction of a ridgeline plot when we view the field lines in cylindrical coordinates (Figure 4a). The periodic nature of the fieldline is then apparent (Figure 4b). The oscillation of the ridgeline can be attributed to an area preserving deformation of the magnetic surface as the fieldline precesses around it and its *fundamental period* is the poloidal period of the fieldline.

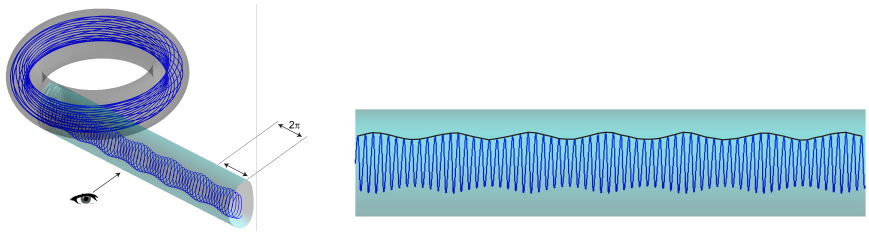


(*a*) (*b*)

Fig. 4: (a) The original toroidal geometry containing a single fieldline for multiple toroidal windings in Cartesian coordinates superimposed with the same geometry in Cylindrical coordinates. (b) The ridgeline plot of maximal points is shown in black and has a period of 10.

To extract the fundamental period of a ridgeline plot, which is essentially a 1D function we make use of a Yin Estimator [3] which minimizes the following difference:

$$\min_{f \in N}(\sigma) = \sum_{i=0}(r_i - r_{i+f})^2 \tag{8}$$

where $r_i$ is the local maxima from equation 7, and $f$ is the fundamental period.

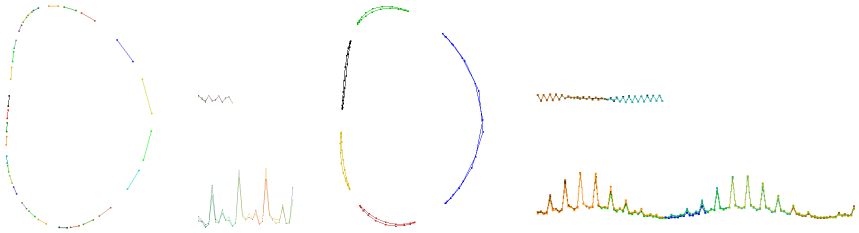

(a) (b) (c) (d)

Fig. 5: (a) A Poincaré section of a 29,11 flux surface. The number of curved sections, 29 corresponds to the toroidal winding number. (b) Top, the ridgeline plot with a period of 11. (b) Bottom, the distance plot with a period of 29. (c) A Poincaré section of a 5,2 island chain. The number of islands, 5 corresponds to the toroidal winding number. (d) Top, the ridgeline plot with a period of 42. (d) Bottom, the distance plot with a period of 105. Each island contains 21 points in its cross-section.

Table 3: Toroidal winding periods via 125 poloidal punctures ranked based on the best period.

| Toroidal Period | Normalized Variance |
|---|---|
| 37 | 0.00255453 |
| 58 | 0.0071927 |
| 29 | 0.00790372 |
| 45 | 0.0177908 |
| 50 | 0.0346803 |
| 53 | 0.0352651 |
| 61 | 0.0433945 |
| 63 | 0.0760976 |
| 42 | 0.0865597 |

Table 4: Poloidal winding period via 46 ridgeline points ranked based on the best period.

| Poloidal Period | Normalized Variance |
|---|---|
| 14 | 1.07227e-05 |
| 22 | 2.48072e-05 |
| 11 | 2.83332e-05 |
| 17 | 6.16752e-05 |
| 20 | 0.000101897 |
| 19 | 0.000105744 |
| 23 | 0.000129318 |
| 16 | 0.000209808 |
| 24 | 0.000210209 |

Table 5: Possible winding pairs found in Table 1 using the periods from Tables 3 and 4 ranking based on an Euclidean distance. [1] reduced to 29,11, [2] discarded

| Winding Pair | Euclidean Distance |
|---|---|
| 37,14 | 0 |
| $58,22^{[1]}$ | 1.41421 |
| $29,11^{[2]}$ | 2.23607 |
| 45,17 | 4.24264 |
| 53,20 | 6.40312 |
| 50,19 | 6.40312 |
| 61,23 | 8.48528 |
| 21,8 | 10.6301 |
| 8,3 | 13.6015 |

## *5.3 Combining Measures*

When analyzing distance measure and ridgeline plots we are able to obtain multiple solutions with different rankings using equations 6 and 8, respectively. For example, in Tables 3 and 4 we show the candidate periods for the distance (toroidal) and ridgeline (poloidal) plots with the descending ranking respectively. Similar periods are seen in Tables 1 and 2 but with different rankings.

While each of the plots yields independent toroidal and poloidal winding periods we now combine them to form the same winding pairs found in Table 1. Further, we rank each pair based on their individual rankings using an Euclidean distance measure (sum of the squares of their individual rankings) (e.g. Table 5).

This ranking results in winding pair 37,14 being the "best" overall approximation having a Euclidean distance of 3.16228 (in Tables 1, 2, and 5 the $37,14$ winding pair was ranked second, fourth, and first respectively thus $\sqrt{1^2+3^2+0^2}$). The resulting

surface is shown in Figure 6. We can use this metric regardless of topology albeit not for chaotic fieldlines.

It is worth noting that the 29,11 winding pair also shows up as 58,22 winding pair (see Table 5). The latter can be reduced to a 29,11 pair as the integers 58,22 have a common denominator of 2. Further, the original 29,11 pair is discarded because its Euclidean ranking distance was greater than the 58,22 pair (Table 5).

Winding pairs that share a common denominator are not unexpected. However, as will be discussed in Section 6, common denominators are a key to differentiating between the topology of flux surfaces and magnetic islands.

Table 6: Winding pairs ranked based on an Euclidean distance.

| Winding Pair | Euclidean Distance |
|---|---|
| 37,14 | 3.16228 |
| 45,17 | 4.12311 |
| 29,11 | 5.09902 |
| 53,20 | 6.78233 |
| 8,3 | 8.30662 |
| 50,19 | 8.77496 |
| 61,23 | 9.43398 |
| 21,8 | 10.0499 |
| 13,5 | 13.3041 |

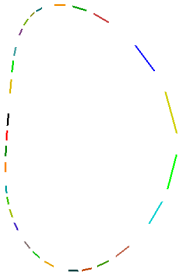

Fig. 6: The best winding pair from Table 6 a 37,14 flux surface with 37 line segments representing the 37 toroidal windings.

## 6 Identifying Island Chains Using Period Estimation

Up to this point we have focused solely on identifying a winding pair that approximates an irrational surface. However, we note that in the case of an island chain an interesting phenomenon occurs.

When analyzing a flux surface, the fundamental periods of the distance and ridgeline plots are *equal* to the toroidal and poloidal winding pair values (Figure 5(b)). While for an island chain, the fundamental periods of the distance and ridgeline plots are *proportional* to the toroidal and poloidal winding pair values (Figure 5(d)). In [12] we showed that the proportionality constant for the ridgeline plot was equal to the number of points in the cross-sectional profile of the island. We have since observed the same for the distance measure plot. This proportionality is due to the periodic nature of the puncture points as well as the periodic nature of the points defining the cross section of the island.

While we have not yet fully investigated, we believe the difference in the proportionality between a flux surface and an island chain is due to the fact that the puncture points in an island chain are topologically separate from each other (i.e. multiple closed curves), while for a flux surface the puncture points will overlap with each other (i.e. one closed curve).

Further, we observed that the number of candidate winding pairs is typically limited as the irrational fieldlines of the island chains continue to reflect the rational fieldlines from which they originated (or broke down) from. For instance, for a 5,2 island chain that utilizes 271 poloidal puncture points and 107 ridgeline points using equation 4 (Section 4.2) results in only one winding pair 5,2 being found.

Constructing the distance measure and ridgeline plots and obtaining the fundamental periods, as shown in Tables 7 and 8, we obtain a "best" winding pair of 105, 42. We can reduce the winding pair to 5,2 by dividing by 21. In the meantime, in Figure 5c, the cross sectional profile of each island is composed of 21 points. In other words, the greatest common denominator of the two periods in the best winding pair obtained using the combined measures of the distance measure and ridgeline plots is larger than 1 for an island chain (typically larger than 3 in order to form a closed shape). On the other hand, this greatest common denominator is usually 1 for a flux surface (see the 37,14 surface in Table 5). This characteristic provides a simple test for determining whether a surface is a flux surface or an island chain. If the "best" fundamental periods of the distance and ridgeline plots are some integer multiples of the toroidal and poloidal periods found by equation 4, then not only is the surface an island chain but the common multiplier (e.g. 21 in the previous example) of these multiples is the number of points in the cross sectional profile of each island.

Table 7: Toroidal winding periods for an island chain via 271 poloidal punctures ranked based on the best period.

| Toroidal Period | Normalized Variance |
|---|---|
| 105 | 0.0001533 |
| 110 | 0.00197257 |
| 100 | 0.00428337 |
| 115 | 0.00836247 |
| 95 | 0.0143386 |
| 120 | 0.0164212 |

Table 8: Poloidal winding period for an island chain via 108 ridgeline points ranked based on the best period.

| Poloidal Period | Normalized Variance |
|---|---|
| 42 | 4.29724e-07 |
| 44 | 4.95931e-06 |
| 40 | 1.14382e-05 |
| 46 | 2.00078e-05 |
| 38 | 3.63677e-05 |
| 48 | 3.85742e-05 |

An alternative way for determining whether a surface is a flux surface or an island chain is by looking at the common denominator for the lists of toroidal periods and poloidal periods, separately. For instance, the common denominators for the candidate toroidal and poloidal periods in Tables 7 and 8 are 5 and 2 respectively, which is exactly the winding pair found from equation 4. The common denominator is due to the resonance nature of the fieldline and is an indication of the island topology. For a flux surface, such as for Tables 3 and 4 no such common denominator other than 1 will be found. As will be shown below, this common denominator property gives us an indication of the type of the resonance of the two functions (and literally the fieldline).

## 7 Results and Discussion

The combined metrics described in Section 5.3 have produced accurate results for our tests so far, failing only when encountering chaotic fieldlines. In addition to identifying flux surfaces and magnetic island chains, the metrics are also used to identify rational surfaces whose fieldlines are truly periodic, $A_0(l_0) = A_{\#T}(l_{\#T})$. However, we have found that our technique is not always able to give a definitive result because as one approaches a rational surface the distance between adjacent points goes to zero, which in turn requires an infinite number of points for the analysis. As the future work, we plan to investigate the analysis of rational surfaces using a limited number of points.

We have also examined the periodicity of separatrices near island chains. In Figure 7, the best rational approximations for the three surfaces are all 2,1. It is purely coincident that all three surfaces had the same approximation as selecting a slightly different starting seed point near separatrix could have resulted in a higher order approximation (i.e a winding pair with larger integers).

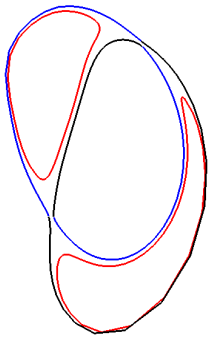

Fig. 7: A 2,1 magnetic island chain (red) surrounded by its separatrices, (blue and black).

In Section 6 two characteristics, i.e. integer multiples and common denominators were discussed which could be used to identify magnetic islands and their unique topology. However, we observed cases where the common denominator did not equal the winding pair found from equation 4. For instance, for a 3,1 island chain that utilizes 278 poloidal puncture points and 91 ridgeline points has a safety factor of 2.99932 while the only winding pair found using equation 4 is 3,1. Constructing distance measure and ridgeline plots and computing the fundamental periods (Tables 9 and 10) we obtain a "best" winding pair of 108, 36. We can reduce the winding pair to 3, 1 by dividing by 36 which is the number of points in the cross sectional profile.

However, unlike our previous island chain example the common denominators for the toroidal and poloidal periods, 18 and 6 respectively, do not equal 3,1. Though they do reduce down to it. This secondary reduction or more precisely secondary resonance, gives further topological information about the island chain. Specifically, the island chain itself contains islands (aka islands within islands). To reduce the common denominators 18,6 to 3,1 an integer multiple of 6 is required. Which is the number of small islands surrounding each island (Figure 8) with each island containing 6 points (i.e. 6 islands with 6 points equaling 36, the number of points in the cross sectional profile).

Finally, we note that we do not compare the present results to our previous geometric tests because they were not a general solution, to the point of being ad-hoc in nature. More importantly they required overlapping puncture points in order to obtain a definitive result. Our new technique gives a definitive result as long as there is a sufficient number of puncture points to perform the period analysis (i.e. at least twice of the fundamental period).

Table 9: Toroidal winding periods for an island chain via 278 poloidal punctures ranked based on the best period.

| Toroidal Period | Normalized Variance |
|---|---|
| 108 | 6.79968e-05 |
| 90 | 0.00092499 |
| 126 | 0.00098725 |
| 144 | 0.00178431 |
| 72 | 0.00195148 |
| 54 | 0.00199423 |
| 36 | 0.00200031 |
| 18 | 0.00201468 |

Table 10: Poloidal winding period for an island chain via 91 ridgeline points ranked based on the best period.

| Poloidal Period | Normalized Variance |
|---|---|
| 36 | variance 3.70173e-07 |
| 30 | variance 4.4525e-06 |
| 42 | variance 4.71553e-06 |
| 48 | variance 9.01227e-06 |
| 18 | variance 1.01154e-05 |
| 24 | variance 1.01895e-05 |
| 12 | variance 1.03454e-05 |
| 6 | variance 1.03557e-05 |

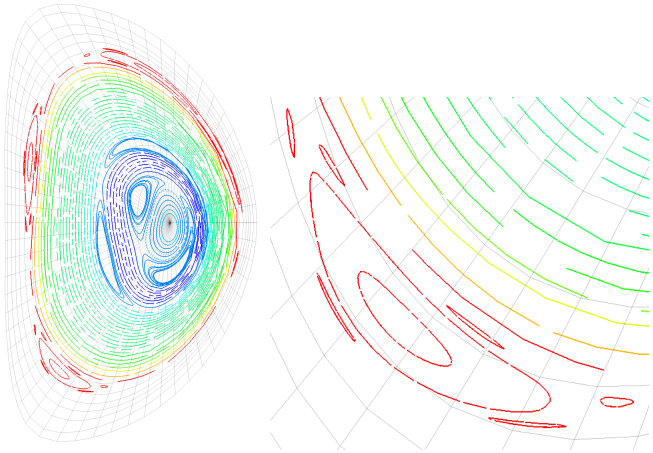

(*a*) (*b*)

Fig. 8: (a) Poincaré plot from a NIMROD simulation of the D3D tokamak. (b) A closeup from the lower left showing the island within islands topology. In this case there are six islands surrounding each of the islands that are part of a 3,1 island chain.

## 8 Summary

In this paper, we discuss the period analysis of the quasi-periodic fieldlines in a toroidal magnetic field. We show that the topology of these fieldlines has direct relationship to the fundamental periods of the distance measure plots and ridgeline plots that are obtained through the computation of fieldlines and Poincaré plot, respectively. We have described how the period analysis of these two plots characterize the behavior of the fieldline. The present framework while having its basis in resonance detection relies on a heuristic solution. Therefore, the future work will focus on the further evaluation of the present combined analysis, and the development of more robust technique for characterizing fieldlines including identifying different topological structures and extracting winding pairs.

**Acknowledgment**

This work was supported in part by the DOE SciDAC Visualization and Analytics Center for Emerging Technology and the DOE SciDAC Fusion Scientific Application Partnership.

## References

1. A. Bagherjeiran and C. Kamath. Graph-based methods for orbit classification. In *In SIAM International Conference on Data Mining*. SIAM, 2005.
2. G. Chen, K. Mischaikow, R. S. Laramee, P. Pilarczyk, and E. Zhang. Vector Field Editing and Periodic Orbit Extraction Using Morse Decomposition. *IEEE Transactions on Visualization and Computer Graphics*, 13(4):769–785, Jul./Aug. 2007.
3. D. Gerhard. Pitch extraction and fundamental frequency: History and current techniques. Technical report, 2003-06.
4. J. M. Green. Locating three-dimensional roots by a bisection method. *Journal of Computational Physics*, 98:194–198, 1992.
5. J. M. Greene. Vortex nulls and magnetic nulls. *Topological Fluid Dynamics*, pages 478–484, 1990.
6. J. Hale and H. Kocak. *Dynamics and Bifurcations*. New York: Springer-Verlag, 1991.
7. R. Laramee, H. Hauser, L. Zhao, and F. H. Post. Topology Based Flow Visualization: The State of the Art. In *Topology-Based Methods in Visualization (Proceedings of Topo-in-Vis 2005)*, Mathematics and Visualization, pages 1–19. Springer, 2007.
8. H. Löffelmann, T. Kucera, and M. E. Gröller. Visualizing poincare maps together with the underlying flow. In *In International Workshop on Visualization and Mathematics '97*, pages 315–328. Springer-Verlag, 1997.
9. R. Peikert and F. Sadlo. Visualization Methods for Vortex Rings and Vortex Breakdown Bubbles. In A. Y. K. Museth, T. Möller, editor, *Proceedings of the 9th Eurographics/IEEE VGTC Symposium on Visualization (EuroVis'07)*, pages 211–218, May 2007.
10. R. Peikert and F. Sadlo. Flow topology beyond skeletons: Visualization of features in recirculating flow. In H.-C. Hege, K. Polthier, and G. Scheuermann, editors, *Topology-Based Methods in Visualization II*, pages 145–160. Springer, 2008.
11. F. H. Post, B. Vrolijk, H. Hauser, R. S. Laramee, and H. Doleisch. The State of the Art in Flow Visualization: Feature Extraction and Tracking. *Computer Graphics Forum*, 22(4):775–792, Dec. 2003.
12. A. Sanderson, G. Chen, X. Tricoche, D. Pugmire, S. Kruger, and J. Breslau. Analysis of recurrent patterns in toroidal magnetic fields. *IEEE Transactions on Visualization and Computer Graphics*, 16:1431–1440, 2010.
13. H. Theisel, T. Weinkauf, H.-P. Seidel, and H. Seidel. Grid-Independent Detection of Closed Stream Lines in 2D Vector Fields. In *Proceedings of the Conference on Vision, Modeling and Visualization 2004 (VMV 04)*, pages 421–428, Nov. 2004.
14. WD.D'haeseleer, W. G. Hitchon, J.D.Callen, and J.L.Shohet. *Flux Coordinates and Magnetic Field Structure, A Guide to a Fundamental Tool of Plasma Theory*. New York: Springer-Verlag, 1991.
15. T. Wischgoll and G. Scheuermann. Detection and Visualization of Closed Streamlines in Planar Fields. *IEEE Transactions on Visualization and Computer Graphics*, 7(2):165–172, 2001.
16. T. Wischgoll and G. Scheuermann. Locating Closed Streamlines in 3D Vector Fields. In *Proceedings of the Joint Eurographics - IEEE TCVG Symposium on Visualization (VisSym 02)*, pages 227–280, May 2002.